Environmental Science: Atmospheres

ROYAL SOCIETY OF CHEMISTRY

PAPER

View Article Online
View Journal | View Issue

Cite this: *Environ. Sci.: Atmos.*, 2022, **2**, 1170

Emission of primary bioaerosol particles from Baltic seawater†

Gabriel P. Freitas, [ab] Christian Stolle,‡[cd] Paul H. Kaye,[e] Warren Stanley,[e] Daniel P. R. Herlemann, [f] Matthew Edward Salter [ab] and Paul Zieger *[ab]

Bioaerosols are particles of biological origin with various important atmospheric implications, for example, within cloud formation where bioaerosols can act as cloud condensation or ice nuclei. Their sources and properties, however, are poorly understood. We conducted a controlled sea spray experiment to determine the properties and emission of primary biological aerosol particles (PBAP) originating from Baltic seawater. Using a single-particle fluorescence and light-scattering instrument, the Multiparameter Bioaerosol Spectrometer (MBS), we differentiated PBAP within sea spray aerosol (SSA). Overall, approximately 1 in 10^4 particles larger than 0.8 μm in diameter were classified as PBAP. The optically-determined morphology of the nascent and fluorescent SSA particles showed a clear transition in symmetry and elongation most likely due to changes in the biogeochemical properties of the surface water. These shifts were also reflected in a clear change of the bacterial community composition of the aerosol and seawater as determined by 16S rRNA-gene analysis, which were significantly distinct from each other, suggesting a preferential emission of specific bacteria to the atmosphere. Our results demonstrate the capability of the MBS to identify and count PBAP within SSA on a single-particle basis and will help to better constrain the emission of marine PBAP and their dependence on the seawater's biogeochemical properties.

Received 24th April 2022
Accepted 7th August 2022

DOI: 10.1039/d2ea00047d

rsc.li/esatmospheres

Environmental significance

Bioaerosol particles emitted from the ocean are important for our environment and climate with a variety of different biological, chemical and physical aspects, for example, by being involved in the formation of cloud ice and precipitation. Within a controlled chamber experiment, we investigated their physical and optical properties, their microbial composition and determined their contribution to sea spray aerosol emissions. The novel approach presented here will help to better constrain their presence and significance within the atmosphere and their overall role in climate.

1 Introduction

Marine primary biological aerosol particles (PBAP) are biological particles which are ejected directly from the ocean within sea spray aerosol (SSA).[1] They are comprised of biological entities such as bacteria, viruses, small fungi and algae or the biologically functional particles derived from them such as spores and pollen.[2] These particles are emitted into the atmosphere as single cells, fragments and as agglomerates of more cells or cells attached to other particles. PBAP and bioaerosols in general are important for climate since they interact with solar radiation and are involved in cloud formation. Bioaerosols

[a]*Department of Environmental Science, Stockholm University, Stockholm, Sweden. E-mail: paul.zieger@aces.su.se*

[b]*Bolin Centre for Climate Research, Stockholm, Sweden*

[c]*Leibniz Institute for Baltic Sea Research Warnemünde, Rostock, Germany*

[d]*Institute for Chemistry and Biology of the Marine Environment, University of Oldenburg, Wilhelmshaven, Germany*

[e]*Centre for Atmospheric and Climate Physics Research, University of Hertfordshire, Hatfield, UK*

[f]*Center of Limnology, Estonian University of Life Sciences, Tartu, Estonia*

† Electronic supplementary information (ESI) available: The document includes details on the auxiliary aerosol size spectrometers; data processing; concentration calculations; description of laboratory experiments; shiptrack of the EMB184 campaign; experimental setup of the SSSC; photos of EMB184 campaign; overview of the particle size distributions of nascent sea spray; fluorescence spectra of EMB184 particle classes; timeline of particle classes contribution; period size-resolved particle classes contribution; table of PBAP and HFSSA contribution to coarse mode per size; comparison between EMB184 and laboratory experiments size distribution; particle classes classification of laboratory experiments; comparison of the fluorescence spectra from the different retrieved groups to literature values; timelines of various aerosol, seawater and ambient parameters; comparison between integral normalized number size distributions for coarse particles and fluorescent particles, HFSSA and PBAP; list of chamber water samples; contribution of microbial classes collected on particle filters and chamber water samples; relation of indicator organisms. See https://doi.org/10.1039/d2ea00047d

‡ Current address: Project Management Jülich, Rostock, Germany.

are known to be efficient ice nucleating particles (INP) and cloud condensation nuclei[3] and are expected to contribute significantly to the INP concentrations above marine regions.[4] INP concentrations have experimentally been linked to water biological activity.[5] In turn, ice crystal concentrations in mixed phase clouds can influence various cloud properties such as cloud phase, albedo and lifetime.[6] Thus, quantifying the emission of PBAP from marine sources is important to improve our ability to predict the phase of clouds, along with precipitation and climate forcing within models.[1]

Over oceans, PBAP are primarily released into the atmosphere as a small fraction of SSA which is one of the largest natural aerosol sources in terms of mass.[7,8] SSA is a complex mixture of inorganic salts and organic matter.[9] The production of SSA is driven by the interaction of wind with the surface of the ocean which causes air entrainment in the form of bubbles and subsequent bubble bursting leading to droplet release into the atmosphere. These can either be film droplets formed by the bursting of the bubble film or jet droplets formed by the projection of droplets after the collapse of the bubble cavity. The first are smaller and more numerous while the latter are larger and less abundant.[9,10]

The sea surface microlayer (SML) is a sub-millimeter thick layer located at the interface between the ocean and atmosphere that is often enriched in both organic matter and microbes compared to the underlying seawater.[11–13] As bubbles rise through the water column they scavenge the organic material concentrated in the SML, emitting this material through bubble bursting.[13,14] Studies suggest that the aerosolization of organic material and microorganisms is quantitatively important but it might be a selective process (*e.g.*, due to differences in their size, surface properties and preferable position in the water column which can influence aerosolization).[15–17]

Offline methods to sample PBAP have been widely employed across different research fields. These approaches usually involve the collection of a particulate sample using filters or impingers and subsequent laboratory analysis such as microscopy or DNA sequencing techniques. While offline techniques reveal important information such as detailed composition, the drawbacks of such methods are particle aging and stress[18] and low time-resolution.[19] Recently, real-time single-particle analysis instruments have been developed based on ultra-violet light-induced fluorescence (UV-LIF).[19–24] UV-LIF methods are tailored around specific wavelengths to probe molecules (*e.g.* tryptophan) present within PBAP while trying to minimize interference from unwanted fluorophores.[25] The main advantage of such methods is a continuous record of PBAP optical properties and concentration.

Recently, several experimental efforts were made to measure PBAP within marine environments[26–28] and in laboratory studies[29,30] combining UV-LIF methods with offline measurements such as filter collection. Other studies have also attempted to determine the role of seawater characteristics on the emission of PBAP.[31,32] While these studies identified links between the seawater biological activity and the emission of PBAP and concentration of INPs, they highlight the need to further assess the source and characteristics of these PBAP and quantify their emissions.

Within this work, we conducted a field experiment to determine the emission and properties of PBAP emitted within nascent SSA generated from Baltic seawater using a sea spray simulation chamber. To do so, we have utilized the single-particle Multiparameter Bioaerosol Spectrometer (MBS)[33] together with filter sampling for bacterial community composition analysis to investigate how the PBAP emissions were impacted by the biological activity in the water.

2 Methods

2.1 Campaign description

The EMB184 campaign took place aboard the R/V *Elisabeth Mann Borgese* (EMB), on the Baltic Sea from the 30th of May to the 11th of June, 2018. A large portion of the cruise was spent taking measurements close to the eastern coast of the Swedish island of Gotland. The ship track is shown in Fig. S1 in the ESI.† The overall objective of the campaign was to study the role of the air-sea interface on the production of marine aerosol particles. The ship was equipped with a flow-through self-cleaning monitoring box (SMB, Leibniz-Institut für Ostseeforschung and 4H-JENA engineering GmbH, Germany) to continuously record the conductivity, temperature, salinity, turbidity and chlorophyll-a content of the seawater entering the sea spray chamber from 5 m depth at the ship's bow.

2.2 Sea spray simulation chamber

The sea spray simulation chamber (SSSC) used to generate nascent SSA particles is described in detail by Salter *et al.*,[34] where bubble surface area, density and air entrainment have been characterized for different sea surface temperatures. The chamber was operated in flow-through-mode by taking water from the ship's seawater supply. The seawater entered the chamber through a plunging jet in the lid of the chamber *via* a peristaltic pump (Watson–Marlow, 620S, U.K.). This plunging jet resulted in the entrainment of air into the seawater inside the SSSC, creating bubbles that subsequently rose to the surface and burst resulting in the formation of SSA particles. The headspace of the SSSC was constantly flushed with particle-free dry air at a rate of 30 lpm using a dry air generator (Kaeser Kompressoren, Dental 1T, KCT110, Germany) equipped with a HEPA filter. The inner walls of the SSSC were coated with Teflon. A second peristaltic pump (Watson–Marlow, 620Di, U.K.) was used to remove seawater from the SSSC at the same rate as the input of water allowing continuous operation of the SSSC with a constant seawater level within. This setup is shown in Fig. S2 and S3.† Its noteworthy that a SML will also form within the SSSC.[11,14] Despite a probable difference in composition to the ambient SML, it can be regarded as one possible composition of a SML.

A conductivity sensor (Aanderaa 4120, Norway) was used to monitor seawater salinity and temperature and a second probe (Aanderaa oxygen optode 4175, Norway) was used to measure

the dissolved oxygen concentration and seawater temperature within the SSSC.

2.3 The Multiparameter Bioaerosol Spectrometer

A MBS (University of Hertfordshire, U.K.)[33] was used to assess the presence of PBAP within nascent sea spray. In brief, the MBS measures the optical size, shape and intrinsic fluorescence of individual particles in real-time. The instrument is a development of the Wideband Integrated Bioaerosol Spectrometer (WIBS)[21,35] and improvements include higher resolution particle optical scattering pattern and fluorescence emission spectra excited at 280 nm excitation wavelength. The MBS detects and sizes each particle in a narrow (1 mm) diameter aerosol sample flow using a low-power (8 mW) visible laser (635 nm). Within this work, particles with optical diameters below 0.8 μm were discarded as they fall below the 50% counting efficiency[36] and the remaining particles were labeled as coarse particles (CP). Following the detection of the particle, a second high-power visible laser (200 mW at 637 nm) is then pulsed to record particle light scattering pattern data using two parallel 512 pixel linear complementary metal–oxide–semiconductor (CMOS) arrays, symmetrically placed at each side of the laser beam. This enables retrieval of information on the particle's size and morphology.[37] Some 30 μs later, a xenon flash-lamp with an excitation wavelength of 280 nm is triggered to excite particle fluorescence, recorded by an 8-channel photomultiplier (PMT) over the spectral range 305 and 655 nm. The total MBS aerosol inlet flow was 3.11 lpm, comprising 0.52 lpm of sample flow containing particles to be measured and the remainder passing through a HEPA filter before rejoining the sample flow as a protective sheath of clean air. A silicon diffusion drier was used prior to the instrument to reduce the RH at the inlet to RH < 31% as measured with a temperature and RH probe (Hytelog USB/RS232, B + B Sensors, Germany). The particle sizing of the instrument was verified using polystyrene latex spheres and compared to auxiliary optical particle size spectrometer measurements (Fig. S4†).

So-called forced trigger (FT) cycles of the MBS were periodically performed in the absence of particles (by switching off the air pump) to remove the instrument's background fluorescence noise levels. Each FT cycle comprised 42 xenon lamp triggers, with background fluorescence being collected. The mean of this signal for each PMT channel was then subtracted from the subsequent particle fluorescence measurements. Furthermore, each individual channel signal from the MBS detector was subtracted by 3 times the background standard deviation (3γ). Negative values were clipped to 0. Here, CP particles with fluorescent signal (FL) greater than this threshold at one of the 8 fluorescence channels were classified as fluorescent particles (FP) and particles with fluorescence signal greater than 9γ were classified as highly fluorescent, further details follow in section 3.1. A series of so-called 'shape parameters' were automatically determined using the MBS software based upon the CMOS arrays data. One of these was the so-called asymmetry factor (AF) that represents the degree of asymmetry between the left and right CMOS array scattering signal. In principle, high AF values, on a scale 0–100, represent more irregularly shaped rough surfaced particles while lower AF values represent more regularly shaped particles that scatter with greater azimuthal uniformity. Another shape parameter is the so-called peak-to-mean ratio (PTMR) that represents the highest light scattering value recorded within an array divided by the mean signal across the whole array. This is done for both the right and left side CMOS arrays. High PTMR values can be interpreted as belonging to elongated or fiber-like particles.[38] The rate at which particles can be optically characterized in this way is ultimately limited by the recharge time of the xenon flash-lamp (6 ms). This effectively limits the maximum rate of analysis to approximately 160 particles per second, meaning for particle sampling rates higher than this, some particles will be counted but not analyzed. Given this limitation, the instrument outputs two metrics: total particle number (*total*), which are those particles counted and sized by the first low-power laser, and measured particle number (*measured*), which is the number of particles for which fluorescence and shape properties have been determined using the xenon flash lamp and high-power laser. We have considered the difference between these two metrics *e.g.* when calculating the actual concentration of PBAP or of fluorescent particles in general (see ESI†).

2.4 Collection and analyses of the bacterial community composition

Water samples from the SSSC were taken in 8 hours-intervals. Bacteria were collected by filtering 500 mL tank water onto polycarbonate filter (Whatman, 0.22 μm, 47 mm). Aerosolized bacteria were collected from the headspace of the sea spray simulation chamber. To do so, a pump-generated air-flow (1.6 lpm) was guided through a filtering device, holding a polycarbonate filter (Whatman, 0.22 μm, 47 mm). Filters were exchanged every 8 hours. After filtration (water samples) or collection (aerosol samples), all filters were frozen in liquid N_2 and stored at −80 °C until further processing. Extraction of DNA from the filters was done by a phenol/chloroform extraction method modified from Weinbauer *et al.*[39] All DNA-extracts were quantified using the Quant-iTTM PicoGreenTM dsDNA assay (Thermo Fisher Scientific, Darmstadt, Germany). The bacterial 16S rRNA gene was amplified using primers covering the V3–V4 region, modified from Herlemann *et al.*[40] Amplicon PCR, Index PCR, quantity and quality control and sequencing of the individual libraries as pool in one Illumina MiSeq run was performed by an external provider (LGC Genomics, Berlin, Germany). The sequences were quality checked using Trimmomatic (V0.36) to remove illumina-specific sequences and regions with low-sequence quality (average quality score < Q20). In addition, PCR primers were removed using cutadapt (V2.3). The reads were paired (16 bp overlap, minimum length 300 bp) and quality trimmed using the VSEARCH tool.[41] These were then taxonomically assigned using the SILVA next-generation sequencing (ngs) pipeline[42] based on SILVAngs analysis platform release version 138.[43] SILVAngs analysis platform performs additional quality checks according to SINA-based alignments[44] with a curated seed database in which PCR

artifacts or non-SSU reads are excluded. SILVAngs analysis platform was able to classify a total of 4 488 410 sequences. Non-bacterial sequences such as chloroplasts, mitochondria, eukaryotes, and archaea were excluded because the primer set employed in the analysis only has very limited coverage of these groups (3 320 422 sequences). The raw reads supporting this study are openly available at the European Nucleotide Archive Project PRJEB49421 (Accession number ERA7898138).

Among all the analyzed samples the SILVAngs analysis platform classified the sequences to 864 operational taxonomic units (OTUs) on genus level. The number of reads per sample varied between 173048–9165 sequences per sample. Given the large variation in the data it was normalized by cumulative sum scaling (CSS) using the R package metagenomeSeq.[45] Variations in bacterial community structure were characterized by non-metric multidimensional scaling using the Bray–Curtis dissimilarity in the PAST software package version 3.22.[46] The one-way permutational multivariate analysis of variance (PERMANOVA test) with Bray–Curtis dissimilarity and sequential Bonferroni significance was used to calculate differences between bacterial community composition among analyzed sample groups.

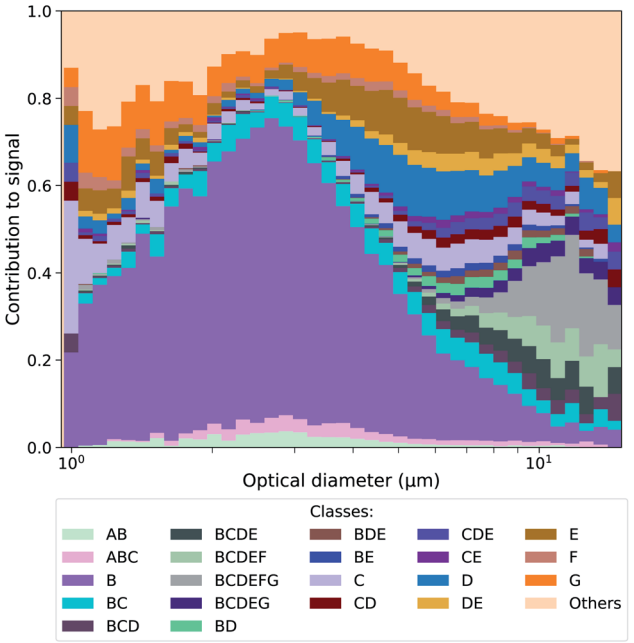

Fig. 1 Contribution of highly fluorescent particle classes *vs.* optical diameter measured during the entire campaign. The results for the corresponding time series and the different periods are shown in the Fig. S6 and S7.†

3 Results and discussion

3.1 Classification of fluorescent particles

Throughout the campaign a constant flux of large FP (optical diameter > 0.8 μm) was observed. Not all FP should be considered as having primary biological origin since interference can come from *e.g.* SSA enriched in organic matter.[25] To further differentiate the classes of FP detected by the MBS, a classification similar to Perring *et al.*[47] was performed. According to Table 1, a particle that exceeded the 9γ fluorescence threshold at one or more channels, was labelled by the corresponding letter(s). For example, a particle that exceeded this threshold at channels 2 and 3 was classified as a BC particle. This approach follows the work by Savage *et al.*,[48] who showed that a 9γ threshold is useful to distinguish PBAP from interfering low fluorescent particles. Particles that exhibited fluorescence lower than 9γ at all channels were collectively classified as fluorescent sea spray aerosol (FSSA). The most abundant classes of particles present during the campaign are shown in Fig. 1 and their corresponding mean fluorescence signal are given in Fig. S5† along with a timeline and period contribution of classes throughout the cruise in Fig. S6 and S7.† In Fig. 1, it is shown that most of the highly fluorescent particle classes within the size range of 0.8–6 μm were class B particles, whereas the larger particles were dominated by particle classes that exceeded the 9γ threshold in more than one channel.

Table 1 Description of the detector channels names, numbers, center wavelength (Cλ) and letters assigned to particles that exceed the 9γ fluorescence threshold at each channel

Channel	Number	Cλ (nm)	Letter
XE1_1	1	315	A
XE1_2	2	364	B
XE1_3	3	414	C
XE1_4	4	461	D
XE1_5	5	508	E
XE1_6	6	552	F
XE1_7	7	595	G
XE1_8	8	640	H

Laboratory sea spray experiments were performed after the campaign to evaluate which classes could potentially contain PBAP. SSA produced from Baltic seawater, a culture medium prepared from filtered Baltic seawater and a pure inorganic sea salt solution were analyzed (see ESI† for a more detailed description of the experiments). No highly fluorescent classes with more than 5 particles were observed in the SSA generated from the inorganic sea salt solution, while some were found for the SSA generated from the culture medium and the Baltic seawater (Fig. S8 and S9†). Strikingly, classes whose highest fluorescence signal was observed in the B channel were only present in the aerosol generated from the Baltic seawater, which is the only aerosol sample where PBAP are expected to be found. Other particle classes (mainly with signals in the C, D, E and F channels) were found in both the seawater and the filtered seawater, showing that those particles were probably sea spray particles coated with water soluble organics.

These laboratory findings are in line with results by Santander *et al.*[30] and justify our approach that highly fluorescent particle classes with a maximum signal in the B channel were grouped as PBAP, and the remaining particles, as highly fluorescent sea spray aerosol (HFSSA). A visualization of this decision tree is given in Fig. 2. The FSSA group generally showed very weak fluorescence

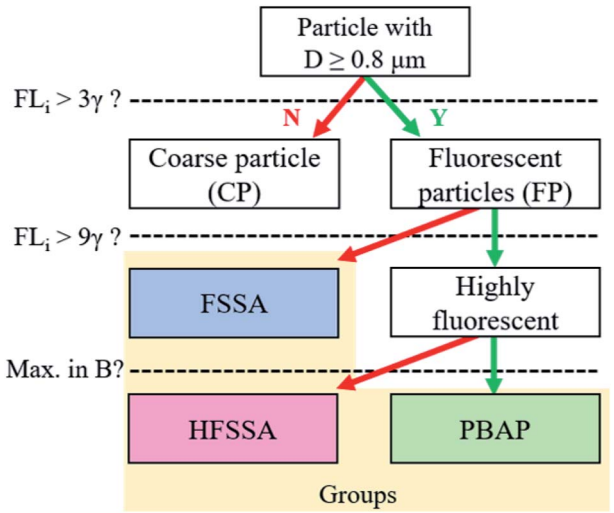

Fig. 2 Decision tree for classification of fluorescent particles. Particles with diameters larger than 0.8 μm and with a fluorescent signal exceeding the 3γ-threshold at any detector channel are labelled as fluorescent particles (FP). FP whose fluorescent signal exceeds 3γ but not the 9γ-threshold are grouped as fluorescent sea spray aerosol (FSSA). Those that exceed the 9γ threshold are grouped as highly fluorescent sea spray aerosol (HFSSA) or as primary biological aerosol particles (PBAP) if their maximum fluorescent signal is observed in the B channel.

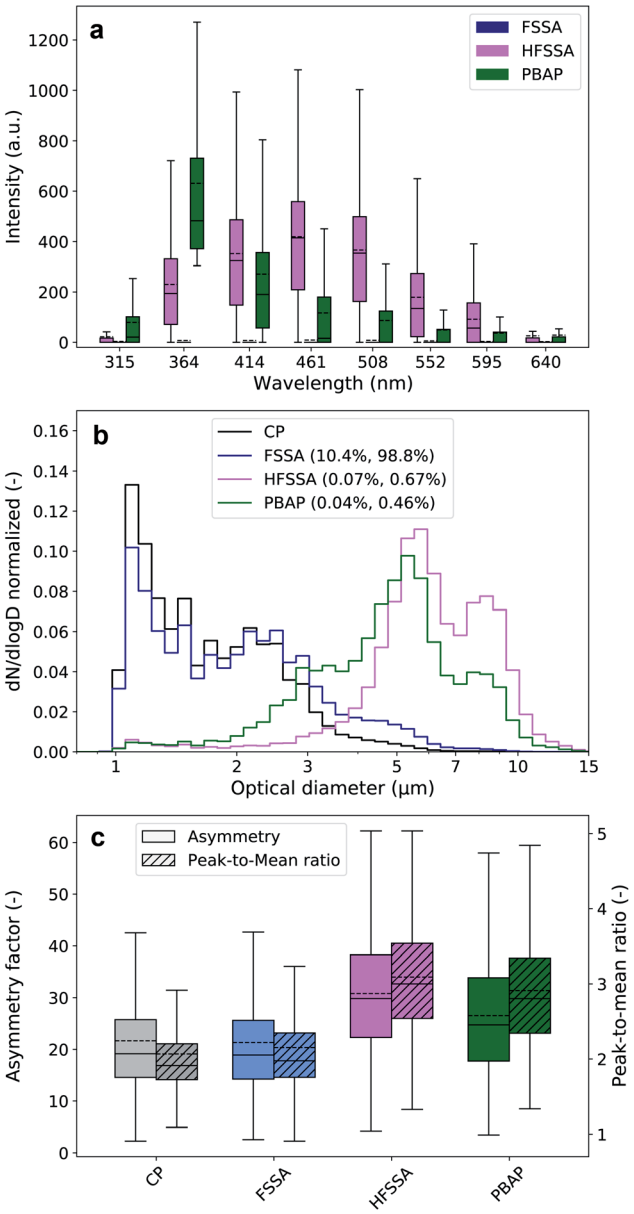

Fig. 3 Result of decision tree classification of all fluorescent particles. (a) Fluorescence spectra of the different fluorescent particle groups. (b) Integral-normalized size distributions with their overall contribution to the measured coarse particles and fluorescent particles given in the legend, respectively. The black line denotes the normalized size distribution of all coarse particles (CP). (c) The asymmetry and peak-to-mean ratio of fluorescent groups and all CP.

in all channels (Fig. 3a) since they fall below the 9γ-threshold. They also shared a similar size distribution (Fig. 3b) and shape parameters (Fig. 3c) as the non-fluorescent CP, while comprising 10.4% of all CP and up to 98.8% of the FP. The dominance of faintly fluorescing particles has been observed previously by Crawford *et al.*,[49] where 97.7% of the FP exhibited such fluorescence behavior. The fluorescence spectra of the HFSSA most likely resembles that of water-soluble organic compounds excited at 280 nm,[50] although the emission wavelengths of these fluorophores can depend on other parameters such as pH.[50] HFSSA is represented by large particles (mean size, 5.9 μm, see Fig. 3b) which are often more asymmetrical and elongated than FSSA (mean asymmetry and peak-to-mean ratio of 30.8 and 3.1, respectively, see Fig. 3c). It is probable that these particles are larger SSA particles coated with increased amounts of fluorescent organic molecules leading to a very broad and high fluorescence emission signal with no particular defined peak and diverse morphology. Santander *et al.*[30] used excitation emission matrix spectroscopy (EEMS) to show that SSA particles emitted from filtered seawater retain this characteristic emission, further strengthening our classification.

PBAP are characterized by a very distinctive fluorescence signal which closely resembles the tryptophan fluorescence emission spectra at the excitation wavelength of 280 nm[25]. This clearly suggests that these particles may have a biological origin. Furthermore, the corresponding size distribution is centered at 5 ± 2 μm which is similar to the size of bacteria agglomerates previously identified in both ambient coastal aerosol[51] and nascent SSA generated in laboratory experiments.[18,30] Interestingly, a number of recent studies suggest that PBAP constitutes only a small portion of the FP over or close to marine environments[27,49] and our data would appear to corroborate this: the PBAP contribution to the total FP was only 0.46% (0.04% of all CP).

A comparison of our identified groups with the excitation emission matrix spectroscopy (EEMS) spectra with a 280 nm excitation wavelength of SSA extracts by Santander *et al.*[30] is shown in Fig. S10.† The characteristics of the PBAP group we have identified resemble that of the bacterial isolates measured by Santander *et al.*[30] Further, this group exhibits a peak in

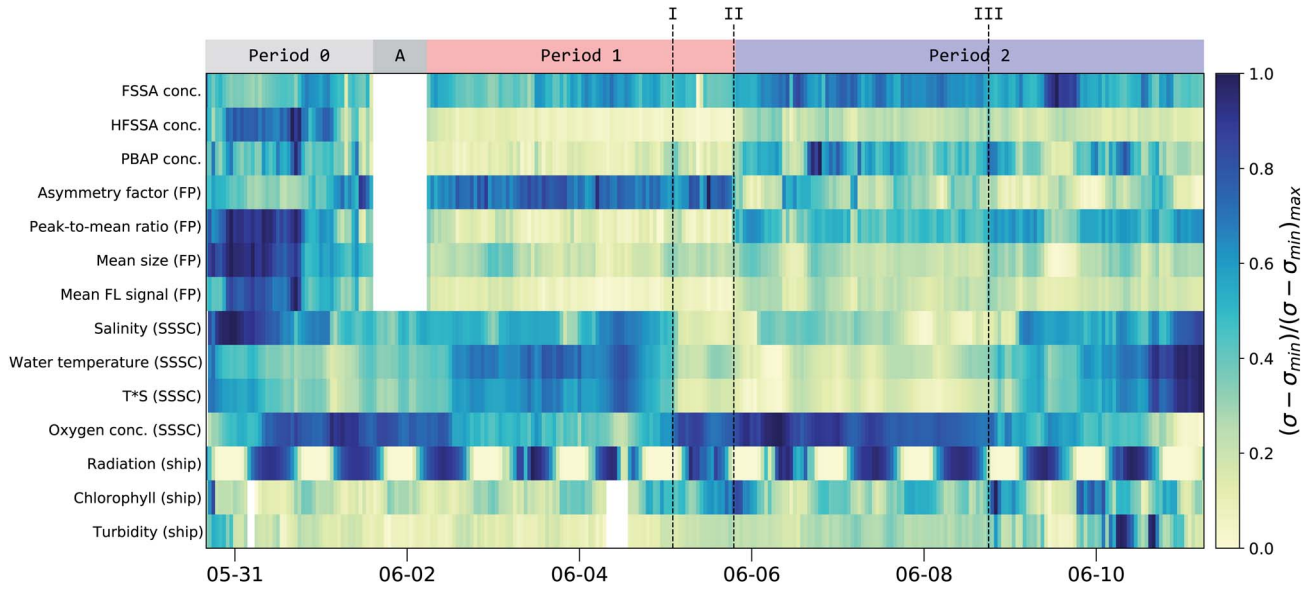

Fig. 4 Normalized concentration of the fluorescent particle groups along with key parameters from the seawater and the solar radiation. The normalized concentration is calculated by subtracting the minimum value from the 1 hour mean values ($\sigma - \sigma_{min}$) and dividing by the new maximum value $(\sigma - \sigma_{min})_{max}$. The corresponding range (max/min-values) are given in Table 2. At the top, the main periods are indicated and timestamps of interest are given in roman numerals (see text). Period 0 refers to MBS measurements within the SSSC prior to the collection of particle filters. Period A indicates a period when the MBS was not connected to the SSSC, while period 1 and 2 are times when the MBS was sampling from the SSSC. See Fig. S11† in the ESI for individual curves.

fluorescence at around 360 nm which is similar to the nascent SSA measured by the same authors with a peak at around 330 nm. Santander *et al.*[30] observed that this peak became much less prominent in the SSA produced from filtered seawater suggesting that the particles within this group are much more likely to be large PBAP than SSA containing predominantly fluorescent dissolved organic matter. The observed spectral shift in comparison to Santander *et al.*[30] could be explained by differences in the instrumental spectral resolution and the general variability of the analyzed biological fluorophores.[25,52]

3.2 Changes in seawater and aerosol properties during the campaign

An overview of the main parameters of the campaign is shown in Fig. 4 as a normalized timeline achieved by subtracting the minimum value (σ_{min}) and then dividing by the new maximum value $(\sigma - \sigma_{min})_{max}$. The corresponding minimum and maximum values together with further average statistical values are given in Table 2. Timelines showing the evolution of each individual parameter in an absolute scale is given in Fig. S11.†

Since the MBS is based on single-particle detection, re-sampling of the data to retrieve particle concentrations was required (see ESI†). Parameters from the SSSC sensors (oxygen, temperature and salinity of the seawater within the chamber), ship's weather station and SMB module were also re-sampled to hourly mean values.

Comparison of the MBS and seawater data allowed the identification of three distinct periods throughout the campaign (Fig. 4) along with 3 points of interest (I, II and III). At the beginning of the campaign (Period 0, P0) the MBS measured aerosols generated in the SSSC prior to the collection of particle filters. During period A the MBS was not connected to the SSSC. During period 1 (P1) and period 2 (P2) continuous filter and water samples were taken from the SSSC in parallel with the MBS measurements. P1 and P2 showed distinct differences in filter, water and MBS data, as will be described below.

The interplay between dissolved oxygen and the water salinity and temperature can be seen in Fig. 4. This was expected, as oxygen solubility is dependent on these factors.[53] There was also an inverse relation between solar radiation and chlorophyll-a content of the water due to diurnal depth fluctuations of microorganisms.[54] Chlorophyll-a is often regarded as a proxy for biological activity, and consequently, biological emission from ocean surfaces. However, recent findings suggest this may not be the case.[55] Indeed, during the campaign, chlorophyll-a was not correlated to MBS-based estimates of PBAP emissions for the entire period (correlation coefficient or *r*-value of 0.22). However, past point III, there is a slight increase in the correlation between PBAP and chlorophyll-a (*r*-value of 0.63) along with an increase in correlation between PBAP and turbidity (*r*-value of 0.71).

There is a clear difference between P1 and P2 in the PBAP concentration (5.6 and 14.6 $\times 10^{-3}$ cm^{-3}, respectively; see green curve in Fig. 5). An abrupt morphology change of the FP was observed (point II in Fig. 4) with more asymmetrical and rough surfaced particles in P1 and more elongated particles in P2 compared to P1. Interestingly, there is a clear difference in particle classes composition between these two periods, as shown in Fig. S6 and S7† in the ESI, further illustrating this differentiation. This sudden change in particle shape could

Table 2 Overview of fluorescent and coarse mode particle properties (MBS retrieval), seawater parameters and solar radiation measured throughout the entire experiment. The minimum (Min), first quartile (Q1), median, mean, third quartile (Q3) and maximum (Max) values are calculated for hourly re-sampled geometric mean values

Parameter	Min	Q1	Median	Mean	Q3	Max	Unit
Coarse particles (CP) conc.	8.98	21.7	24.9	25.0	28.5	40.2	cm^{-3}
Contribution of fluorescent particles (FP) to CP	8	9.71	10.5	10.7	11.1	15.6	%
Fluorescent sea spray (FSSA) concentration	0.8	2.2	2.6	2.6	2.9	4.1	cm^{-3}
Highly fluorescent sea spray (HFSSA) conc.	1.7	7.9	13.1	16.4	18.5	64	10^{-3} cm^{-3}
Contribution of HFSSA to CP	0.01	0.03	0.05	0.08	0.07	0.44	%
Primary biological aerosol particles (PBAP) conc.	1.9	6.1	11.8	11.8	16	30	10^{-3} cm^{-3}
Contribution of PBAP to CP	<0.01	0.02	0.05	0.05	0.07	0.22	%
Asymmetry factor[a]	16	18.2	19.7	20	22	25	—
Peak-to-mean ratio[a]	1.88	1.95	2.07	2.05	2.12	2.30	—
Mean size[a]	1.79	1.96	2.01	2.0	2.09	2.62	µm
Mean FL signal[a]	37.4	50.3	57.4	63.4	67.1	148	a.u.
Salinity[b]	6.62	6.87	7.04	7.01	7.12	7.45	g_{salt} per kg_{water}
Water temperature[b]	12.7	13.75	14.4	14.5	15.4	16.8	°C
Temperature·salinity[b]	87	94	102	102	109	123	°C·g_{salt} per kg_{water}
Oxygen[b]	258	274	281	279	285	292	mM l^{-1}
Solar irradiation[c]	<0.1	14.7	1242	1193	2258	2706	W m^{-2}
Chlorophyll-a[d]	0.45	0.91	1.18	1.29	1.55	2.96	$mg_{Chl\text{-}a}$ m^{-3}_{water}
Turbidity[d]	0.42	0.45	0.48	0.49	0.5	0.715	NTU

[a] Of all fluorescent particles. [b] Measured within the sea spray simulation chamber. [c] Measured by ship's weather station. [d] Measured by the ship SMB module.

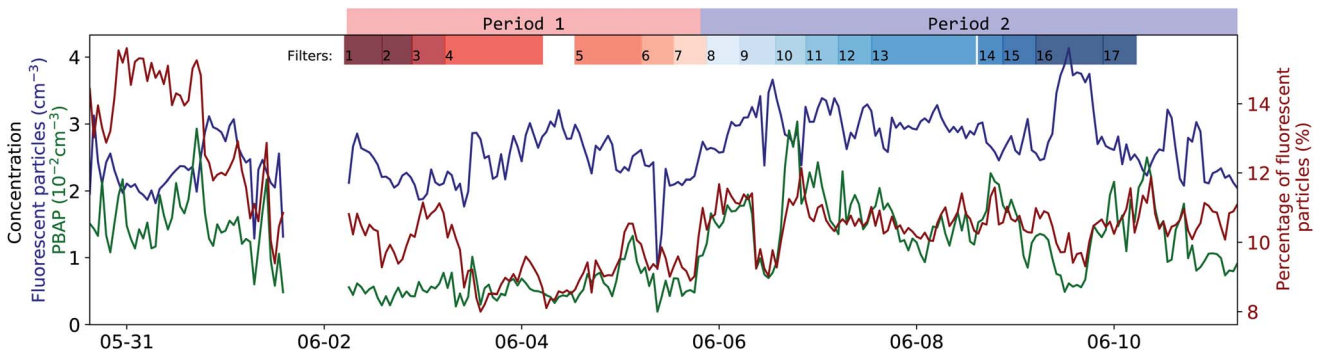

Fig. 5 Time series of the concentration of fluorescent particles and the PBAP group. Blue curve: concentration of all fluorescent particles (particles >0.8 µm in optical diameter and fluorescence signal larger than 3γ of the background). Green curve: concentration of PBAP. Red curve: relative contribution of fluorescent particles to all detected particles with >0.8 µm (in %). The periods of filter sampling for microbial community analysis are shown on top of the graph (length corresponds to the filter sampling time) along with the separation between the two morphology periods.

have been due to changes in the water composition leading to differences in the chemical and biological sea spray composition. Such relation has been previously reported by Kaluarachchi *et al.*[56] This change occurred after an abrupt gradient in the temperature times salinity (*T***S*) curve (point I) which suggests a change in water mass. A particularly high chlorophyll-a concentration peak is present right before the morphology transition occurred (point II) on the first day in which this concentration remained high even during high radiation periods. Also noteworthy was that past point III a new water mass was observed (*T***S* curve) along with a peak in FSSA concentrations, while chlorophyll-a, PBAP, turbidity and mean size reached very low levels.

As shown in Fig. S1,† P1 represents a time-span when the ship was close to the island of Gotland while P2 experienced more open waters in the middle of the Gotland-Latvia strait. Such geographical differences might explain the differences in physical and chemical properties of the sampled seawater.

3.3 Concentration and contribution dynamics of fluorescent and primary biological particles

The concentration of FP (retrieved using eqn (1)† given in the ESI, see blue curve Fig. 5) had an almost constant level of around 2.2 cm^{-3} for most of the campaign. With only slightly notable lower concentrations at the beginning and a distinct peak during filter 16 in P2. The contribution of FP to the entire CP population was around 9.71–11.1% (interquartile range, see red curve Fig. 5), which in relative terms increased with particle size (see Fig. S12a† in SI, *e.g.*, at around 5.5 μm, 50% of the particles were classified as FP). This size dependency for the contribution of FP to CP could be explained by the fact that as SSA particles get larger, they are more likely to contain enough fluorophore material to surpass the 3γ fluorescence threshold. The continuous flux of SSA particles generated by the SSSC had an almost constant particle size distribution where only the concentration is inversely proportional to water temperature, see Fig. S4† in ESI and Salter *et al.*[57] for further details.

The concentration of PBAP (see green curve in Fig. 5) does not strictly follow the same time dependency as the FP (which mostly consists of FSSA), indicating that their rate of emission could have been governed by different factors such as the microbial community composition and their dispersion through the water column inside the SSSC. Generally, the concentration ranged between 6.1 and 16 $\times$ 10^{-3} cm^{-3} (interquartile range). Interestingly, during P2 the PBAP concentration followed closely the percentage of FP within CP, even when FP concentrations were high and the percentage is low (Filter 16, P2). This may suggest that the amount of PBAP (*e.g.* bacteria) in the water can influence the availability of organic fluorophores that coat and cause fluorescent SSA particles.

The herein calculated concentrations are experiment specific and characteristic of a combination of seawater physiochemical properties, such as temperature and dissolved matter. Although the biogeochemical properties of the SML inside the SSSC might differ from the SML present at the air-sea interface, our experiment is still likely to provide a reasonably good model for the emission of PBAP from fresh seawater. The entrainment of air within the SSSC has been characterized and shown to reflect natural entrainment and bubble area density due to wind sheer.[34] The PBAP concentrations presented here are a first estimation but are in a similar range as PBAP emissions found within SSA using filter based methods.[58] Furthermore, it is estimated that INP constitute approximately 1 in every 10^5–10^6 particles in the atmosphere.[5,59] Given that we expect PBAP to be efficient INP,[3–5] we also expect PBAP populations to be present at similar concentrations. Indeed, with our experiment we identified PBAP to be approximately 1 in every 10^4 particles above 0.8 μm which lies in the same range as expected INP concentrations in marine environments (keeping in mind that the number size distribution of SSA particles is dominated by sub-micron particles which are not detected by the MBS, see Fig. S4†).

It is difficult to directly determine the PBAP emission flux from our observations due to the general challenge of upscaling laboratory sea spray chamber experiments. However, it is possible to give a first estimate of the PBAP flux using a selected sea spray source function (see *e.g.* Salter *et al.*[57] or Grythe *et al.*[60]) in combination with the size-resolved contribution of PBAP (or HFSSA) to coarse mode aerosol that we present here (see Fig. S12 and Table S1† in the ESI).

3.4 Bacterial community composition

Along the top of Fig. 5 the collection of 17 aerosol filter samples (AFS) within the SSSC is shown. In addition, chamber water samples (CWS) were collected at 8 hours intervals and the collection times are provided in Table S2.†

The most abundant operational taxonomic units (OTU) in the aerosol and water samples belonged to the classes Gammaproteobacteria, Alphaproteobacteria, Bacteroidia, Actinobacteria and Oxyphotobacteria in order (Fig. S13 and S14†). On this phylogenetic level the following differences between AFS and CWS communities were minor: the relative contribution of Alphaproteobacteria were higher in the CWS, whereas the

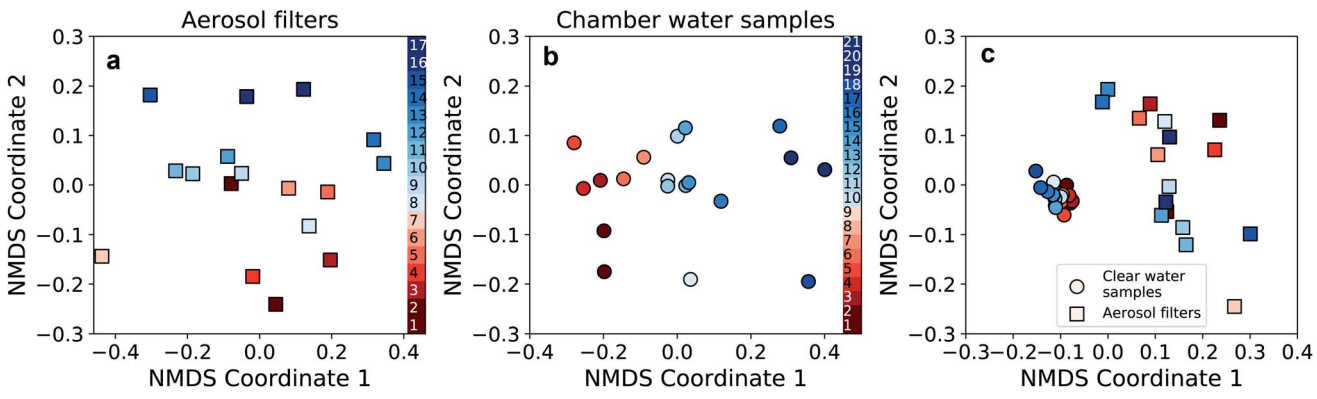

Fig. 6 Non-metric multidimensional scaling (NMDS) analysis of the aerosol filter and chamber water samples. (a) NMDS performed on the bacterial community data of the aerosol filter samples (stress: 0.171). (b) NMDS analysis on the bacterial community data of the chamber water samples (stress: 0.156). For (a) and (b), samples are color-coded chronologically within period P1 (red colors) and P2 (blue colors, see Fig. 5). (c) Combined NMDS analysis of the bacterial community composition of the aerosol (squares) and water (circles) samples (stress 0.110; same color-code as in panel a and b).

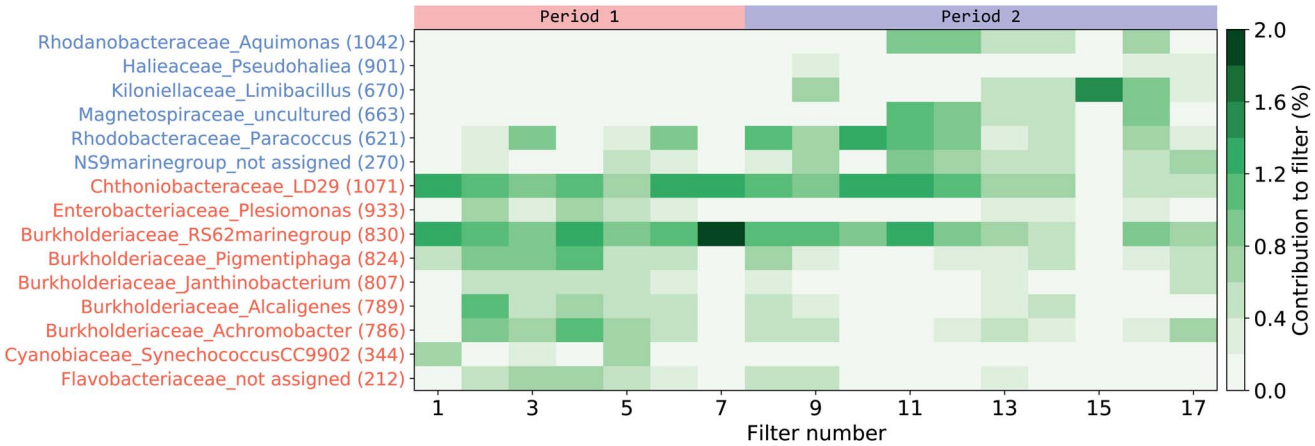

Fig. 7 Indicator organism (IO) analysis of the aerosol filter samples. Organisms pointed out by the LEfSe analysis as characterizing either the first (red indicator organism (IO) numbers) or the second period (blue IO numbers) have their contribution per filter signal shown. For full taxonomy classification refer to Table S3† in the ESI.

relative contribution of Gammaproteobacteria were higher in the AFS. This was also reflected in the mean ratio between Gammaproteobacteria and Alphaproteobacteria which was 1.01 and 1.47 for CWS and AFS, respectively. The dynamics of the community composition on class level between periods P1 and P2 was only small. The mean ratio between Gammaproteobacteria and Alphaproteobacteria during P1 was 1.14 for CWS and 1.80 for AFS. During P2, this decreased to 0.98 and 1.28 for CWS and AFS, respectively.

In order to compare CWS and AFS in more detail at the OTU-level, the bacterial community composition was visualized using non-metric multidimensional scaling (NMDS). Communities in aerosol and water samples showed differences between the two periods (*i.e.*, P1 and P2), which, however, were statistically significant only for the CWS community (PERMANOVA, $p < 0.01$). Nevertheless, these differences between P1 and P2, especially in the CWS bacterial community, reflect the observed changes in most parameters throughout the campaign (Fig. 6a and b). Furthermore, at the OTU-level, the community compositions of water and aerosol were consistently different (Fig. 6c, PERMANOVA $p < 0.01$). Implying a selective aerosolization of seawater microorganisms which has been observed previously.[15,16]

A LEfSe analysis[61] was performed on the AFS data to identify potential indicator organisms (IO) that would represent periods P1 or P2 (Fig. 7, Table S3†), that is, organisms that would be prominently present in either period and could be enhanced or depleted due to differences in seawater mass and/or organic content of the SSA. Interestingly, some of the IO in our study have also been previously reported in aerosolized seawater or atmospheric samples during experimental or field studies. Some OTUs from P1 were phylogenetically related to Burkholderiaceae (IO 824), Flavobacteriaceae (IO 212), or Chthoniobacteriaceae (IO 1071), which were also found in atmospheric samples from the Baltic Sea coast close to our study site[15] as well as in aerosols generated from seawater.[32] Likewise, one OTU from P2 was phylogenetically related to Rhodobacteraceae (IO 621), which were also found in aerosol samples from the Western Baltic Sea[62] and in aerosols generated from natural seawater.[16,32] All IO accounted only little to the overall community, with a maximum relative abundance of 2% for one OTU phylogenetically related to the Burkholderiaceae (IO 830 - RS62 marine group).

4 Summary and conclusions

We have shown that the MBS is able to distinguish PBAP from fluorescent and non-fluorescent SSA particles above 0.8 μm (optical diameter). Since not all bioaerosols are expected to be fluorescent at the excitation wavelength used by the MBS, the PBAP concentrations found (ranging between 10^{-3}–10^{-2} cm^{-3}) should be treated as a lower limit. Nonetheless, our findings are in good agreement with previous estimates[58] of atmospheric prokaryotic concentration over oceans which range between 10^{-3} to 10^{-2} cm^{-3}.

PBAP were estimated to constitute only 0.46% of the entire fluorescent particle population. Thus, special care should be taken when using the fluorescence signal to determine concentrations or emissions of marine PBAP. Other UV-LIF instruments with lower spectral resolution might be limited in differentiating between PBAP and fluorescent SSA particles potentially inducing errors when using their data as a proxy for PBAP. We have shown that the MBS spectral resolution of 8 emission channels is especially useful when classifying particles using the 9γ threshold. This method has the advantage of circumventing the use of UV-LIF libraries of known fluorescent particles needed for supervised learning. The diversity in technical details between the used instrumentation, differences in the particle production and treatment (*e.g.* drying) and the lack of a proper calibration material make the creation of the libraries needed for supervised learning methods difficult.[52]

Clear particle morphology changes were observed throughout the experiment that coincided with changes in sampling locations and differences in the physical and chemical properties of the sampled seawater. In agreement with previous studies, our results imply that the changes in seawater

composition lead to differences in the biological and organic composition of the emitted SSA particles[63] with potential impacts on the particle morphology[56] that in turn could potentially influence their ice nucleating propensity.[64]

A distinction into two discrete sampling periods was made based upon changes in the fluorescent particle classes detected by the MBS and this distinction was supported through offline analysis of the bacterial community composition of particle and seawater samples. For the offline analysis, this differentiation was more pronounced in the community composition of the water samples, but was slightly (although not significantly) reflected in the aerosolized community. The aerosolized bacterial community generally differed from its source community in the seawater, supporting previous findings that bacterial aerosolization is a selective process.[15,16] However, the exact underlying mechanism warrants further studies. In addition, the distinction between the two periods allowed the identification of aerosolized bacterial taxa, which were specifically abundant in one of these periods. The low abundance of these indicator organisms hinders a clear link to the dynamics observed in the MBS data and points towards the need for further study details such as the identification of aerosolized bacteria, the degree of their selective transfer, their fate and metabolic activity in the atmosphere.

Overall, our results demonstrate the strength of the MBS in identifying and characterizing individual particles of biological origin, making it a valuable asset for deployment in future experiments to better comprehend and quantify the emission of PBAP across different marine and continental environments. One promising future experiment would be to link single-particle PBAP measurements from the MBS to online INP measurements[65] to shed further light on the interplay between different seawater masses, PBAP, ice nucleating propensity, SSA emissions and their morphology.

Author contributions

CS, MS and PZ were responsible for conceptualization, data curation, investigation, resources and funding acquisition. GF, CS, DH and PZ performed formal analysis. CS, PK, WS, DH, MS and PZ developed the methodology. GF did the visualization of the main figures. PZ was responsible for the supervision. All authors took part in the validation. GF, CS, DH, MS and PZ performed the writing of the original draft. All authors contributed to the review and editing of the manuscript.

Conflicts of interest

There are no conflicts to declare.

Acknowledgements

This work was supported by the Swedish Research Council (Vetenskapsrådet starting grant, project number 2018-05045 and project number 2016-05100). We acknowledge the support from the Leibniz Institute for Baltic Sea Research Warnemünde (IOW). CS received funding from the Leibniz Association SAW in the project 'Marine biological production, organic aerosol particles and marine clouds: a Process Chain (MarParCloud)' (SAW-2016-TROPOS-2). DH was supported by the European Regional Development Fund/Estonian Research Council funded 'Mobilitas Plus Top Researcher grant MOBTT24'. We thank the crew for their excellent technical support during the EMB184 cruise. We thank Julika Zinke (ACES) for her help in setting up the laboratory experiments and preparing the samples and Douglas Nilsson (ACES) for technical support.

References

1 V. R. Després, J. Alex Huffman, S. M. Burrows, C. Hoose, A. S. Safatov, G. Buryak, J. Fröhlich-Nowoisky, W. Elbert, M. O. Andreae, U. Pöschl and R. Jaenicke, Primary biological aerosol particles in the atmosphere: A review, *Tellus B*, 2012, **64**(1), 15598.

2 J. Fröhlich-Nowoisky, C. J. Kampf, B. Weber, J. A. Huffman, C. Pöhlker, M. O. Andreae, N. Lang-Yona, S. M. Burrows, S. S. Gunthe, W. Elbert, H. Su, P. Hoor, E. Thines, T. Hoffmann, V. R. Després and U. Pöschl, Bioaerosols in the Earth system: Climate, health, and ecosystem interactions, *Atmos. Res.*, 2016, **182**, 346–376.

3 Y. Tobo, A. J. Prenni, P. J. Demott, J. A. Huffman, C. S. McCluskey, G. Tian, C. Pöhlker, U. Pöschl and S. M. Kreidenweis, Biological aerosol particles as a key determinant of ice nuclei populations in a forest ecosystem, *J. Geophys. Res.: Atmos.*, 2013, **118**, 100–110.

4 T. W. Wilson, L. A. Ladino, P. A. Alpert, M. N. Breckels, I. M. Brooks, J. Browse, S. M. Burrows, K. S. Carslaw, J. A. Huffman, C. Judd, W. P. Kilthau, R. H. Mason, G. McFiggans, L. A. Miller, J. J. Najera, E. Polishchuk, S. Rae, C. L. Schiller, M. Si, J. V. Temprado, T. F. Whale, J. P. Wong, O. Wurl, J. D. Yakobi-Hancock, J. P. Abbatt, J. Y. Aller, A. K. Bertram, D. A. Knopf and B. J. Murray, A marine biogenic source of atmospheric ice-nucleating particles, *Nature*, 2015, **525**, 234–238.

5 P. J. DeMott, T. C. Hill, C. S. McCluskey, K. A. Prather, D. B. Collins, R. C. Sullivan, M. J. Ruppel, R. H. Mason, V. E. Irish, T. Lee, C. Y. Hwang, T. S. Rhee, J. R. Snider, G. R. McMeeking, S. Dhaniyala, E. R. Lewis, J. J. Wentzell, J. Abbatt, C. Lee, C. M. Sultana, A. P. Ault, J. L. Axson, M. D. Martinez, I. Venero, G. Santos-Figueroa, M. D. Stokes, G. B. Deane, O. L. Mayol-Bracero, V. H. Grassian, T. H. Bertram, A. K. Bertram, B. F. Moffett and G. D. Franc, Sea spray aerosol as a unique source of ice nucleating particles, *Proc. Natl. Acad. Sci. U. S. A.*, 2016, **113**, 5797–5803.

6 B. J. Murray, D. O'sullivan, J. D. Atkinson and M. E. Webb, Ice nucleation by particles immersed in supercooled cloud droplets, *Chem. Soc. Rev.*, 2012, **41**, 6519–6554.

7 D. C. Blanchard, *Air-Sea Exchange of Gases and Particles*, Springer Netherlands, Dordrecht, 1983, pp. 407–454.

8 N. S. Holmes, A review of particle formation events and growth in the atmosphere in the various environments and

discussion of mechanistic implications, *Atmos. Environ.*, 2007, **41**, 2183–2201.

9 D. C. Blanchard, The electrification of the atmosphere by particles from bubbles in the sea, *Prog. Oceanogr.*, 1963, **1**, 73–202.

10 E. R. Lewis and S. E. Schwartz, *Sea Salt Aerosol Production: Mechanisms, Methods, Measurements and Models*, American Geophysical Union (AGU), 2004, ch. 2, pp. 9–99.

11 M. Cunliffe, R. C. Upstill-Goddard and J. C. Murrell, Microbiology of aquatic surface microlayers, *FEMS Microbiol. Rev.*, 2011, **35**, 233–246.

12 A. Engel, H. W. Bange, M. Cunliffe, S. M. Burrows, G. Friedrichs, L. Galgani, H. Herrmann, N. Hertkorn, M. Johnson, P. S. Liss, P. K. Quinn, M. Schartau, A. Soloviev, C. Stolle, R. C. Upstill-Goddard, M. van Pinxteren and B. Zäncker, The Ocean's Vital Skin: toward an Integrated Understanding of the Sea Surface Microlayer, *Front. Mar. Sci.*, 2017, **4**, 165.

13 J. Y. Aller, M. R. Kuznetsova, C. J. Jahns and P. F. Kemp, The sea surface microlayer as a source of viral and bacterial enrichment in marine aerosols, *J. Aerosol Sci.*, 2005, **36**, 801–812.

14 T. B. Robinson, O. Wurl, E. Bahlmann, K. Jürgens and C. Stolle, Rising bubbles enhance the gelatinous nature of the air-sea interface, *Limnol. Oceanogr.*, 2019, **64**, 2358–2372.

15 C. Fahlgren, Å. Hagström, D. Nilsson and U. L. Zweifel, Annual variations in the diversity, viability, and origin of airborne bacteria, *Appl. Environ. Microbiol.*, 2010, **76**, 3015–3025.

16 J. M. Michaud, L. R. Thompson, D. Kaul, J. L. Espinoza, R. A. Richter, Z. Z. Xu, C. Lee, K. M. Pham, C. M. Beall, F. Malfatti, F. Azam, R. Knight, M. D. Burkart, C. L. Dupont and K. A. Prather, Taxon-specific aerosolization of bacteria and viruses in an experimental ocean-atmosphere mesocosm, *Nat. Commun.*, 2018, **9**, 2017.

17 J. Rahlff, C. Stolle, H. A. Giebel, N. I. H. Mustaffa, O. Wurl and D. P. Herlemann, Sea foams are ephemeral hotspots for distinctive bacterial communities contrasting sea-surface microlayer and underlying surface water, *FEMS Microbiol. Ecol.*, 2021, **97**, 1–14.

18 J. P. Patterson, D. B. Collins, J. M. Michaud, J. L. Axson, C. M. Sultana, T. Moser, A. C. Dommer, J. Conner, V. H. Grassian, M. D. Stokes, G. B. Deane, J. E. Evans, M. D. Burkart, K. A. Prather and N. C. Gianneschi, Sea spray aerosol structure and composition using cryogenic transmission electron microscopy, *ACS Cent. Sci.*, 2016, **2**, 40–47.

19 J. A. Huffman, A. E. Perring, N. J. Savage, B. Clot, B. Crouzy, F. Tummon, O. Shoshanim, B. Damit, J. Schneider, V. Sivaprakasam, M. A. Zawadowicz, I. Crawford, M. Gallagher, D. Topping, D. C. Doughty, S. C. Hill and Y. Pan, Real-time sensing of bioaerosols: Review and current perspectives, *Aerosol Sci. Technol.*, 2020, **54**, 465–495.

20 V. Agranovski, Z. Ristovski, M. Hargreaves, P. J. Blackall and L. Morawska, Real-time measurement of bacterial aerosols with the UVAPS: Performance evaluation, *J. Aerosol Sci.*, 2003, **34**, 301–317.

21 P. H. Kaye, W. R. Stanley, E. Hirst, E. Foot, K. L. Baxter and S. J. Barrington, Single particle multichannel bio-aerosol fluorescence sensor, *Opt. Express*, 2005, **13**, 3583.

22 A. M. Gabey, M. W. Gallagher, J. Whitehead, J. R. Dorsey, P. H. Kaye and W. R. Stanley, Measurements and comparison of primary biological aerosol above and below a tropical forest canopy using a dual channel fluorescence spectrometer, *Atmos. Chem. Phys.*, 2010, **10**, 4453–4466.

23 T. Könemann, N. Savage, T. Klimach, D. Walter, J. Fröhlich-Nowoisky, H. Su, U. Pöschl, J. Alex Huffman and C. Pöhlker, Spectral Intensity Bioaerosol Sensor (SIBS): An instrument for spectrally resolved fluorescence detection of single particles in real time, *Atmos. Meas. Tech.*, 2019, **12**, 1337–1363.

24 D. Kiselev, L. Bonacina and J. P. Wolf, A flash-lamp based device for fluorescence detection and identification of individual pollen grains, *Rev. Sci. Instrum.*, 2013, **84**, 033302.

25 C. Pöhlker, J. A. Huffman and U. Pöschl, Autofluorescence of atmospheric bioaerosols - Fluorescent biomolecules and potential interferences, *Atmos. Meas. Tech.*, 2012, **5**, 37–71.

26 J. M. Creamean, J. N. Cross, R. Pickart, L. McRaven, P. Lin, A. Pacini, R. Hanlon, D. G. Schmale, J. Ceniceros, T. Aydell, N. Colombi, E. Bolger and P. J. DeMott, Ice Nucleating Particles Carried From Below a Phytoplankton Bloom to the Arctic Atmosphere, *Geophys. Res. Lett.*, 2019, **46**, 8572–8581.

27 A. Moallemi, S. Landwehr, C. Robinson, R. Simó, M. Zamanillo, G. Chen, A. Baccarini, M. Schnaiter, S. Henning, R. L. Modini, M. Gysel-Beer and J. Schmale, Sources, Occurrence and Characteristics of Fluorescent Biological Aerosol Particles Measured Over the Pristine Southern Ocean, *J. Geophys. Res.: Atmos.*, 2021, **126**(11), e2021JD034811.

28 K. Kawana, K. Matsumoto, F. Taketani, T. Miyakawa and Y. Kanaya, Fluorescent biological aerosol particles over the central Pacific Ocean: covariation with ocean-surface biological activity indicators, *Atmospheric Chemistry and Physics Discussions*, 2021, 1–27.

29 M. Nishimura, T. Shimakita, E. Kamiya, Y. Tashiro and K. Kogure, Use of an automatic cell-counting system with LED illumination for enumeration of marine bacteria, *Fish. Sci.*, 2006, **72**, 723–727.

30 M. V. Santander, B. A. Mitts, M. A. Pendergraft, J. Dinasquet, C. Lee, A. N. Moore, L. B. Cancelada, K. A. Kimble, F. Malfatti and K. A. Prather, Tandem Fluorescence Measurements of Organic Matter and Bacteria Released in Sea Spray Aerosols, *Environ. Sci. Technol.*, 2021, **55**(8), 5171–5179.

31 K. A. Hultin, R. Krejci, J. Pinhassi, L. Gomez-Consarnau, E. M. Martensson, Å. Hagström and E. D. Nilsson, Aerosol and bacterial emissions from Baltic Seawater, *Atmos. Res.*, 2011, **99**, 1–14.

32 C. Harb, J. Pan, S. Devilbiss, B. Badgley, L. C. Marr, D. G. Schmale and H. Foroutan, Increasing Freshwater Salinity Impacts Aerosolized Bacteria, *Environ. Sci. Technol.*, 2021, **55**, 5731–5741.

33 S. Ruske, D. O. Topping, V. E. Foot, P. H. Kaye, W. R. Stanley, I. Crawford, A. P. Morse and M. W. Gallagher, Evaluation of

machine learning algorithms for classification of primary biological aerosol using a new UV-LIF spectrometer, *Atmos. Meas. Tech.*, 2017, **10**, 695–708.

34 M. E. Salter, E. D. Nilsson, A. Butcher and M. Bilde, On the seawater temperature dependence of the sea spray aerosol generated by a continuous plunging jet, *J. Geophys. Res.: Atmos.*, 2014, **119**, 9052–9072.

35 P. H. Kaye, J. E. Barton, E. Hirst and J. M. Clark, Simultaneous light scattering and intrinsic fluorescence measurement for the classification of airborne particles, *Appl. Opt.*, 2000, **39**, 3738.

36 A. M. Gabey, W. R. Stanley, M. W. Gallagher and P. H. Kaye, The fluorescence properties of aerosol larger than 0.8 μ in urban and tropical rainforest locations, *Atmos. Chem. Phys.*, 2011, **11**, 5491–5504.

37 P. H. Kaye, Spatial light-scattering analysis as a means of characterizing and classifying non-spherical particles, *Meas. Sci. Technol.*, 1998, **9**, 141–149.

38 Z. Ulanowski, E. Hirst, P. H. Kaye and R. Greenaway, Retrieving the size of particles with rough and complex surfaces from two-dimensional scattering patterns, *J. Quant. Spectrosc. Radiat. Transfer*, 2012, **113**, 2457–2464.

39 M. G. Weinbauer, I. Fritz, D. F. Wenderoth and M. G. Höfle, Simultaneous extraction from bacterioplankton of total RNA and DNA suitable for quantitative structure and function analyses, *Appl. Environ. Microbiol.*, 2002, **68**, 1082–1087.

40 D. P. Herlemann, M. Labrenz, K. Jürgens, S. Bertilsson, J. J. Waniek and A. F. Andersson, Transitions in bacterial communities along the 2000 km salinity gradient of the Baltic Sea, *ISME J.*, 2011, **5**, 1571–1579.

41 T. Rognes, T. Flouri, B. Nichols, C. Quince and F. Mahé, VSEARCH: A versatile open source tool for metagenomics, *PeerJ*, 2016, **2016**, 1–22.

42 F. O. Glöckner, P. Yilmaz, C. Quast, J. Gerken, A. Beccati, A. Ciuprina, G. Bruns, P. Yarza, J. Peplies, R. Westram and W. Ludwig, 25 years of serving the community with ribosomal RNA gene reference databases and tools, *J. Biotechnol.*, 2017, **261**, 169–176.

43 E. Pruesse, C. Quast, K. Knittel, B. M. Fuchs, W. Ludwig, J. Peplies and F. O. Glöckner, SILVA: A comprehensive online resource for quality checked and aligned ribosomal RNA sequence data compatible with ARB, *Nucleic Acids Res.*, 2007, **35**, 7188–7196.

44 E. Pruesse, J. Peplies and F. O. Glöckner, SINA: Accurate high-throughput multiple sequence alignment of ribosomal RNA genes, *Bioinformatics*, 2012, **28**, 1823–1829.

45 J. N. Paulson, O. Colin Stine, H. C. Bravo and M. Pop, Differential abundance analysis for microbial marker-gene surveys, *Nat. Methods*, 2013, **10**, 1200–1202.

46 Ø. Hammer, D. A. T. Harper and P. D. Ryan, PAST: Paleontological Statistics Software Package for Education and Data Analysis, *Palaeontol. Electron.*, 2001, **4**, 1–9.

47 A. E. Perring, J. P. Schwarz, D. Baumgardner, M. T. Hernandez, D. V. Spracklen, C. L. Heald, R. S. Gao, G. Kok, G. R. McMeeking, J. B. McQuaid and D. W. Fahey, Airborne observations of regional variation in fluorescent aerosol across the United States, *J. Geophys. Res.: Atmos.*, 2015, **120**, 1153–1170.

48 N. J. Savage, C. E. Krentz, T. Könemann, T. T. Han, G. Mainelis, C. Pöhlker and J. Alex Huffman, Systematic characterization and fluorescence threshold strategies for the wideband integrated bioaerosol sensor (WIBS) using size-resolved biological and interfering particles, *Atmos. Meas. Tech.*, 2017, **10**, 4279–4302.

49 I. Crawford, M. Gallagher, K. Bower, T. Choularton, M. Flynn, S. Ruske, C. Listowski, N. Brough, T. Lachlan-Cope, Z. Fleming, V. Foot and W. Stanley, Real Time Detection of Airborne Bioparticles in Antarctica, *Atmospheric Chemistry and Physics Discussions*, 2017, 1–21.

50 R. M. Duarte, C. A. Pio and A. C. Duarte, Synchronous scan and excitation-emission matrix fluorescence spectroscopy of water-soluble organic compounds in atmospheric aerosols, *J. Atmos. Chem.*, 2004, **48**, 157–171.

51 B. Lighthart, The ecology of bacteria in the alfresco atmosphere, *FEMS Microbiol. Ecol.*, 1997, **23**, 263–274.

52 M. Hernandez, A. E. Perring, K. McCabe, G. Kok, G. Granger and D. Baumgardner, Chamber catalogues of optical and fluorescent signatures distinguish bioaerosol classes, *Atmos. Meas. Tech.*, 2016, **9**, 3283–3292.

53 W. Xing, M. Yin, Q. Lv, Y. Hu, C. Liu and J. Zhang, *Oxygen Solubility, Diffusion Coefficient, and Solution Viscosity*, Elsevier B.V., 2014, pp. 1–31.

54 M. D. Ohman, Behavioral responses of zooplankton to predation, *Bull. Mar. Sci.*, 1988, **43**, 530–550.

55 P. K. Quinn, T. S. Bates, K. S. Schulz, D. J. Coffman, A. A. Frossard, L. M. Russell, W. C. Keene and D. J. Kieber, Contribution of sea surface carbon pool to organic matter enrichment in sea spray aerosol, *Nat. Geosci.*, 2014, **7**, 228–232.

56 C. P. Kaluarachchi, V. W. Or, Y. Lan, C. K. Madawala, E. S. Hasenecz, D. R. Crocker, C. K. Morris, H. D. Lee, K. J. Mayer, J. S. Sauer, C. Lee, G. Dorce, F. Malfatti, E. A. Stone, C. D. Cappa, V. H. Grassian, K. A. Prather and A. V. Tivanski, Size-Dependent Morphology, Composition, Phase State, and Water Uptake of Nascent Submicrometer Sea Spray Aerosols during a Phytoplankton Bloom, *ACS Earth Space Chem.*, 2022, **6**(1), 116–130.

57 M. E. Salter, P. Zieger, J. C. Acosta Navarro, H. Grythe, A. Kirkeväg, B. Rosati, I. Riipinen and E. D. Nilsson, An empirically derived inorganic sea spray source function incorporating sea surface temperature, *Atmos. Chem. Phys.*, 2015, **15**, 11047–11066.

58 E. Mayol, J. M. Arrieta, M. A. Jiménez, A. Martínez-Asensio, N. Garcias-Bonet, J. Dachs, B. González-Gaya, S. J. Royer, V. M. Benítez-Barrios, E. Fraile-Nuez and C. M. Duarte, Long-range transport of airborne microbes over the global tropical and subtropical ocean, *Nat. Commun.*, 2017, **8**, 1–8.

59 P. J. DeMott, A. J. Prenni, X. Liu, S. M. Kreidenweis, M. D. Petters, C. H. Twohy, M. S. Richardson, T. Eidhammer and D. C. Rogers, Predicting global atmospheric ice nuclei distributions and their impacts on climate, *Proc. Natl. Acad. Sci. U. S. A.*, 2010, **107**, 11217–11222.

60 H. Grythe, J. Ström, R. Krejci, P. Quinn and A. Stohl, A review of sea-spray aerosol source functions using a large global set of sea salt aerosol concentration measurements, *Atmos. Chem. Phys.*, 2014, **14**, 1277–1297.

61 N. Segata, J. Izard, L. Waldron, D. Gevers, L. Miropolsky, W. S. Garrett and C. Huttenhower, Metagenomic biomarker discovery and explanation, *Genome Biol.*, 2011, **12**, R60.

62 J. S. Seifried, A. Wichels and G. Gerdts, Spatial distribution of marine airborne bacterial communities, *MicrobiologyOpen*, 2015, **4**, 475–490.

63 E. S. Hasenecz, T. Jayarathne, M. A. Pendergraft, M. V. Santander, K. J. Mayer, J. Sauer, C. Lee, W. S. Gibson, S. M. Kruse, F. Malfatti, K. A. Prather and E. A. Stone, Marine Bacteria Affect Saccharide Enrichment in Sea Spray Aerosol during a Phytoplankton Bloom, *ACS Earth Space Chem.*, 2020, **4**, 1638–1649.

64 P. Roy, L. E. Mael, T. C. Hill, L. Mehndiratta, G. Peiker, M. L. House, P. J. Demott, V. H. Grassian and C. S. Dutcher, Ice Nucleating Activity and Residual Particle Morphology of Bulk Seawater and Sea Surface Microlayer, *ACS Earth Space Chem.*, 2021, **5**, 1916–1928.

65 O. Möhler, M. Adams, L. Lacher, F. Vogel, J. Nadolny, R. Ullrich, C. Boffo, T. Pfeuffer, A. Hobl, M. Weiß, H. S. Vepuri, N. Hiranuma and B. J. Murray, The Portable Ice Nucleation Experiment (PINE): A new online instrument for laboratory studies and automated long-term field observations of ice-nucleating particles, *Atmos. Meas. Tech.*, 2021, **14**, 1143–1166.